Article

Impact of Terrigenous Organic Matter Input on Organic Matter Enrichment of Paleocene Source Rocks, Lishui Sag, East China Sea

Xu Han [1,2], Dujie Hou [1,2,*], Xiong Cheng [1,2] and Yan Li [1,2]

[1] School of Energy Resources, China University of Geosciences, Beijing 100083, China
[2] Key Laboratory of Marine Reservoir Evolution and Hydrocarbon Accumulation Mechanism, Ministry of Education, China University of Geosciences, Beijing 100083, China
* Correspondence: houdj313@163.com

Abstract: To clarify the organic matter (OM) enrichment of the Lishui Sag, the factors influencing the variable abundance of OM in the Lingfeng Formation are studied using organic geochemical data. The source rocks of the Lingfeng Formation have medium–high total organic carbon (TOC) values (0.53–3.56%). The main type of kerogen is II2-III. Compared to the shallow marine subfacies source rocks, the TOC of the delta front subfacies source rocks is higher. The distribution of biomarkers shows that the redox environment of the delta front subfacies source rock is the sub-oxidizing and oxic environment, and the source rock is mainly supplied by terrigenous higher plants; the redox environment of shallow marine subfacies source rocks is a sub-reducing and suboxic environment, and the OM mainly comes from algae. The link between OM input and OM abundance demonstrates that terrigenous OM (TOM) input has a considerable influence on OM abundance. However, there is no obvious relationship between preservation and OM abundance, which suggests that preservation is not the determining element in OM enrichment. The strong sediment flux decreases the amount of time that OM is exposed to oxygen. As a result, delta front subfacies with large TOM input have a huge number of excellent source rocks. This paper proposes a "delta front-OM input model" for excellent source rocks.

Keywords: marine source rocks; geochemical characteristics; organic matter enrichment; Lingfeng Formation; Lishui Sag

1. Introduction

The primary prerequisite for the accumulation of hydrocarbons is an abundance of organic materials in the source rocks [1]. Excellent source rocks contribute 80% of oil and gas and control the advantageous transport direction of oil and gas [2,3]. Therefore, determining the organic matter (OM) enrichment mechanism in source rock is an important part of oil and gas exploration and development [4–8]. Over time, a new topic of study has emerged: the enrichment of organic content in marine source rocks. Many successful studies on the organic material enrichment mechanisms of marine source rocks have been carried out [9–11]. OM supply, redox conditions, paleo-salinity fluctuations and paleoclimate control the OM enrichment of marine source rock [12]. OM supply includes primary productivity at the surface of the ocean (plankton and algae) and terrestrial OM input [4,5,13–15]. OM supply is the basis for OM enrichment. Redox conditions have a strong influence on OM preservation [12,16,17]. Reduction conditions are conducive to OM preservation [10,18]. High paleo-salinity is beneficial to OM preservation. The warm and humid paleoclimate favors biological growth [10,18,19]. Large rivers have a strong influence on OM enrichment. Aquatic organisms thrive due to the nutrients brought by rivers [13,20]. Meanwhile, the amount of OM in the water is large because of the terrigenous organic matter (TOM) brought by rivers [20]. However, oxygen is carried by large rivers

into sedimentary waters, causing the sedimentary environment to become an oxidizing environment, which is unfavorable to OM preservation [1,20].

Six oil-bearing structures and one petroleum and natural gas field have been discovered in the study area since the 1990s [21]. The Lishui Sag has become a new focus of exploration. Hydrocarbon accumulation factors in the Lishui Depression have been researched by many scholars. Previous studies have clarified that the Lingfeng Formation (E1l) and the Yueguifeng Formation (E1y) are the primary source rocks, and the petroleum and natural gas are mainly derived from the E1l [21–23]. Trap formation time and passage opening time are all related to the oil and gas charging period [24–26]. Maturation is conducive to sand body development in the gently sloping zone of the western Lishui Sag, and this area is favorable for oil and gas charging and preservation [27–30]. The OM enrichment modes of the Lingfeng and Yueguifeng Formations have also been studied [21,22,31]. However, previous works have mainly focused on the differences between the Lingfeng and Yueguifeng Formations. The Lishui Sag has an excellent drainage system and reservoir sealing conditions. However, during the depositional period of the E1l, the sedimentation rate of the sedimentary facies was rapid [22,24,30]. The location of excellent source rock development changed rapidly. This change led to the differential accumulation of hydrocarbon. There is a paucity of systematic research on the modes of OM enrichment, the primary factors governing the development of excellent source rocks, and the differential accumulation in a single formation. The ambiguous OM enrichment mode of a single interval severely restricts the process of exploration. Therefore, this paper uses E1l source rocks as the research object and employs organic geochemical analyses to establish new source rock evaluation standards that are suitable for the study area. Based on the planar distribution characteristics of excellent source rocks and combined with macroscopic carbon isotope and microscopic biomarker compound analyses, the mechanism of OM enrichment is analyzed. The main factors influencing the development of excellent source rocks are investigated, and finally, an OM enrichment model is established. The location of excellent source rock development is indicated, and theoretical guidance for the next phase of exploration in the Lishui Sag is provided.

2. Geological Setting and Stratigraphy

The Lishui Sag is located in the western East China Sea Shelf Basin (ECSSB) [32,33]. The ECSSB lies at the convergence zone of the Eurasian, Pacific, and Philippine plates. Two uplifts split the Lishui Sag to the west and south (Figure 1) [26,34,35]. The morphology of the Lishui is controlled by the NE-trending segmental faults. The Lingfeng low bulge divides the study region into two parts: western and eastern [21,26,27]. The tectonic evolution phases of the Lishui Sag from the Cretaceous to the Tertiary are impacted by variations in the western Pacific plate's subduction direction and rifting. The tectonic evolution phases of the study area includes a rift stage, a post-rift depression stage, an uplift stage and a regional subsidence stage [23,26,27,29,31].

The stratigraphic column of the study area includes Late Cretaceous, Paleogene, Neogene and Quaternary strata. By integrating biostratigraphic data, conventional core facies, gamma ray (GR) logging facies and seismic facies characteristics, a three-level sequence stratigraphic framework, including six key horizons, namely, T80, T83, T85, T88, T90 and T100, was constructed (Figure 2) [21,28,30]. The primary source rock is the lower Paleocene Yueguifeng Formation (E1y), with the overlying Lingfeng Formation serving as a secondary source rock (E1l) [21,22,26].

During the depositional period of the E1l, three main sedimentary facies developed: fan-delta, delta and shallow marine facies (Figure 2) [21,22,30,31]. The delta plain subfacies are widely developed in the western slope belt of the west subsag, and the delta front subfacies are locally developed in the steep slope belt. The east subsag is controlled by the provenance on both sides of the low Lingfeng Uplift and the Yandang Uplift, and fan-delta facies are widely developed in the eastern part [21,30]. The source rocks of the Lingfeng

Formation can be divided into delta front subfacies (wells A, C, E and F) and shallow marine subfacies source rock (wells B, D and G).
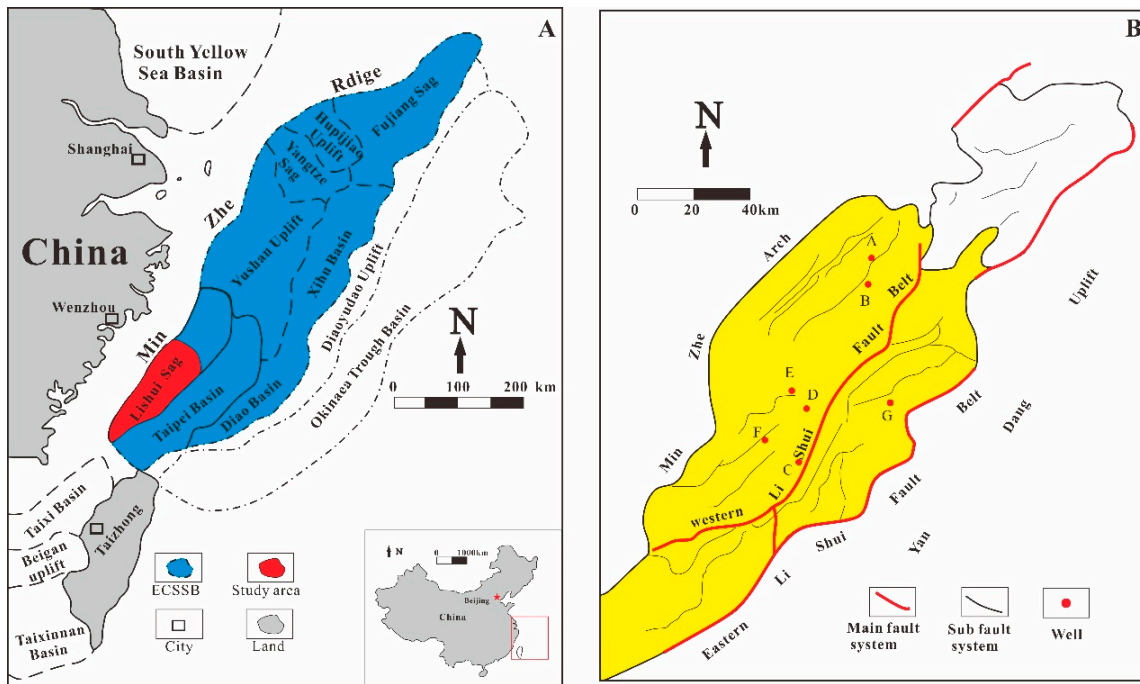

Figure 1. (**A**) Tectonic location of the East China Sea Shelf Basin (ECSSB). (**B**) Structural units of the Lishui Sag. A: Well A; B: Well B; C: Well C; D: Well D; E: Well E; F: Well F; G: Well G.
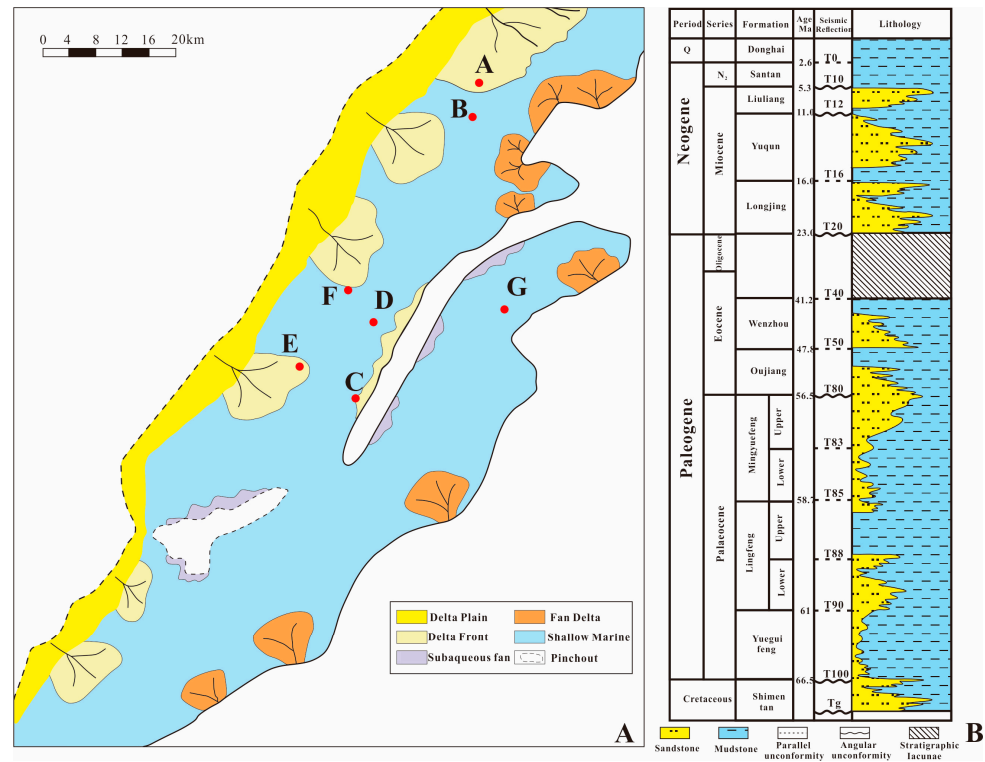

Figure 2. (**A**) Sedimentary subfacies plan of the Lingfeng formation in the Lishui Sag; (**B**) stratigraphic units of the Paleocene in the Lishui Sag. A: Well A; B: Well B; C: Well C; D: Well D; E: Well E; F: Well F; G: Well G.

The lithology of E1l is dominated by gray, dark gray and black mudstones with interbedded thin-layered, light-gray calcareous siltstones, fine sandstones and a few thin-layered calcareous fine sandstones [21,30]. The sandstone gradually changes from fine sand to silt in the upper part, and the calcium content of mudstone increases, forming a positive cycle of coarse grains at the bottom and fine grains at the top [24,25,31]. The calcium content of mudstone decreases downward, and the sandy limestone that contains algae and other bioclasts has an uneven thickness but is distributed in the whole area and can be used as a marker layer. The Shanghai facies mudstone can be continuously tracked in the area and is not at an angle to the underlying strata [21,26–28].

3. Materials and Methods

A total of 119 samples of gray to dark gray delta front–neritic mudstone from the Neo-E1l were collected from seven exploratory wells, namely, A, B, C, D, E, F, and G, in this study. Among them, 76 pieces were samples of rock cuttings, and 43 pieces were samples of rock cores. In this paper, total organic carbon (TOC) analysis, pyrolysis, and biomarker compound analysis were carried out at the China University of Geosciences, Beijing. Before the start of the experiment, 126 samples were cleaned to remove drilling fluid. Then, the best samples were selected for testing.

A total of 119 samples were analyzed for TOC analysis and Rock-Eval pyrolysis. The source rock samples were crushed to 80 mesh. The inorganic carbon was removed using dilute hydrochloric acid. Then, the source rock samples were analyzed using a CS-580A C/S analyzer to estimate the TOC according the GB/T 19145–2003 standard. The samples utilized for the TOC analysis and pyrolysis analysis were processed in the same way. The measured parameters included the TOC, volatile hydrocarbon HC content (S_1), remaining HC generative potential (S_2), and maximum pyrolysis yield temperature (T_{max}). The hydrogen index (HI) was calculated from the TOC and S_2. The parameters were determined using the GB/T 18602-2012 standard as a guide.

A total of 43 rock core samples were used for chloroform extraction and group component separation. All samples were crushed to 80–120 mesh, and 100 g of the samples was placed in a 75 °C water bath for Sox extraction for 72 h. The extracts were recovered by an evaporator to recover chloroform and evaporated to dryness for later use. In accordance with the SY/T5119-2016 standard, the extracts were separated on silica/alumina gel and eluted with n-hexane.

A total of 43 samples of saturated hydrocarbon components were analyzed by gas chromatography–mass spectrometry (Agilent 7890-5975c) with a DB-5MS elastic quartz capillary column (60 m × 0.25 mm × 0.25 μm). The velocity of carrier gas was held constant at 1 mL/min. The carrier gas was 99.999% helium gas, and the temperature at the inlet was 310 °C. The temperature was held constant at 50 °C for 4 min throughout the heating program, and then it was raised to 300 °C at a rate of 4 °C/min and held there for 35 min. The parameters were determined using the GB/T 18606-2001 standard as a guide.

4. Results

4.1. Abundance of Organic Matter

The values of TOC in the E1l are between 0.53 and 3.56%, with an average of 1.16%. The HI values of the source rocks are between 8.14 and 204.59 mg HC/g TOC, with an average of 90.7 mg HC/g TOC. The hydrocarbon generation potential ($S_1 + S_2$) values of the source rocks are between 0.07 and 3.59 mg/g, with an average of 1.41 mg/g (Table S1). In general, the source rocks of the Lingfeng Formation have good potential for producing hydrocarbons.

4.2. Type of Organic Matter

According to the van Krevelen plot of hydrogen index (S_2/TOC X100) and Tmax displayed in Figure 3, the type of OM has been categorized. The figure shows that the kerogen type of the source rock of the E1l is dominated by types II_2–III [36]. Kerogen types

II–III suggest that the source rocks of the E1l have different abilities to produce petroleum and natural gas [37–40]. The source rocks of the E1l are mainly gas-generating, and a small number are oil-generating [41–44].
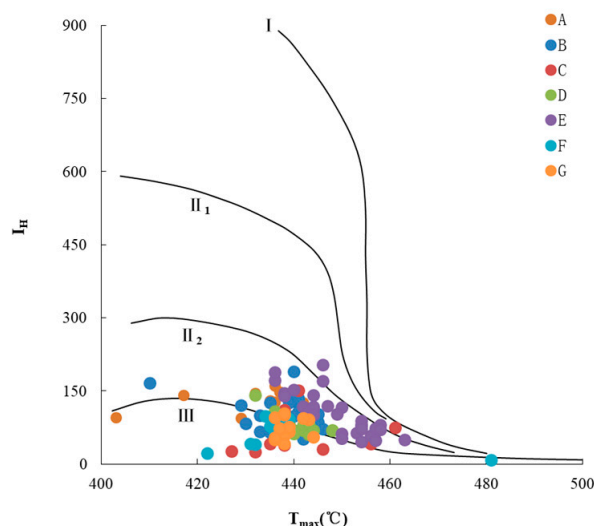

Figure 3. Plot of HI versus Tmax based on rock pyrolysis. A: kerogen type of Well A; B: kerogen type of Well B; C: kerogen type of Well C; D: kerogen type of Well D; E: kerogen type of Well E; F: kerogen type of Well F; G: kerogen type of Well G.

4.3. Molecular Biomarkers

4.3.1. Normal Alkanes and Isoprenoids

The distribution characteristics of n-alkanes in all samples can be divided into three types (Figure 4). The chromatograms of saturated hydrocarbon from the samples of some delta front subfacies source rocks (wells A and F) show a unimodal distribution of alkanes between C_{14} and C_{35}, with an excess of long-chain n-alkanes between C_{27} and C_{33} (Figure 4). The chromatograms of saturated hydrocarbon from the samples of the other delta front subfacies source rock (wells C and E) show a bimodal distribution of alkanes between C_{14} and C_{35}, with an excess of short- and medium-chain n-alkanes between C_{17} and C_{22} and an excess of long-chain n-alkanes between C_{24} and C_{28} (Figure 4). The chromatograms of saturated hydrocarbon from the samples of the shallow marine subfacies source rock (wells B, D and G) show a unimodal distribution of alkanes between C_{14} and C_{33}, with an excess of short- and medium-chain n-alkanes between C_{17} and C_{22} (Figure 4). The pristane/phytane ratio (Pr/Ph) of the delta front subfacies source rocks range from 0.63 to 4.81, with an average of 2.8. The Pr/Ph of the shallow marine subfacies source rocks are between 1.12 and 3.57, with an average of 2.7 (Table 1). The $nC1_{5+17+19}/nC_{27+29+31}$ ratios of the delta front subfacies source rocks range from 0.13 to 5.91, with an average of 0.9 (Table 1). The $nC_{15+17+19}/nC_{27+29+31}$ ratios of the shallow marine subfacies source rocks are 0.59–2.57, with an average of 1.5 (Table 1). The nC_{27+29}/nC_{31+33} ratios of the delta front sub-facies source rocks are between 1.15 and 2.44, with an average of 1.8 (Table 1). The nC_{27+29}/nC_{31+33} ratios of the shallow marine subfacies source rocks are 2.09–3.56, with an average of 2.9 (Table 1). The average chain length (ACL) values of the delta front subfacies source rocks are 24.58–28.35, with an average of 27.2 (Table 1). The ACL values of the shallow marine subfacies source rocks are 25.49–26.75, with an average of 26.2 (Table 1). The aquatic microphyte (Paq) values of the delta front subfacies source rocks are between 0.27 and 0.95, with an average of 0.5 (Table 1). The Paq of the shallow marine subfacies source rocks range from 0.56 to 0.81, with an average of 0.7 (Table 1). The ratio parameters of the biomarker compounds are shown in Table 1.
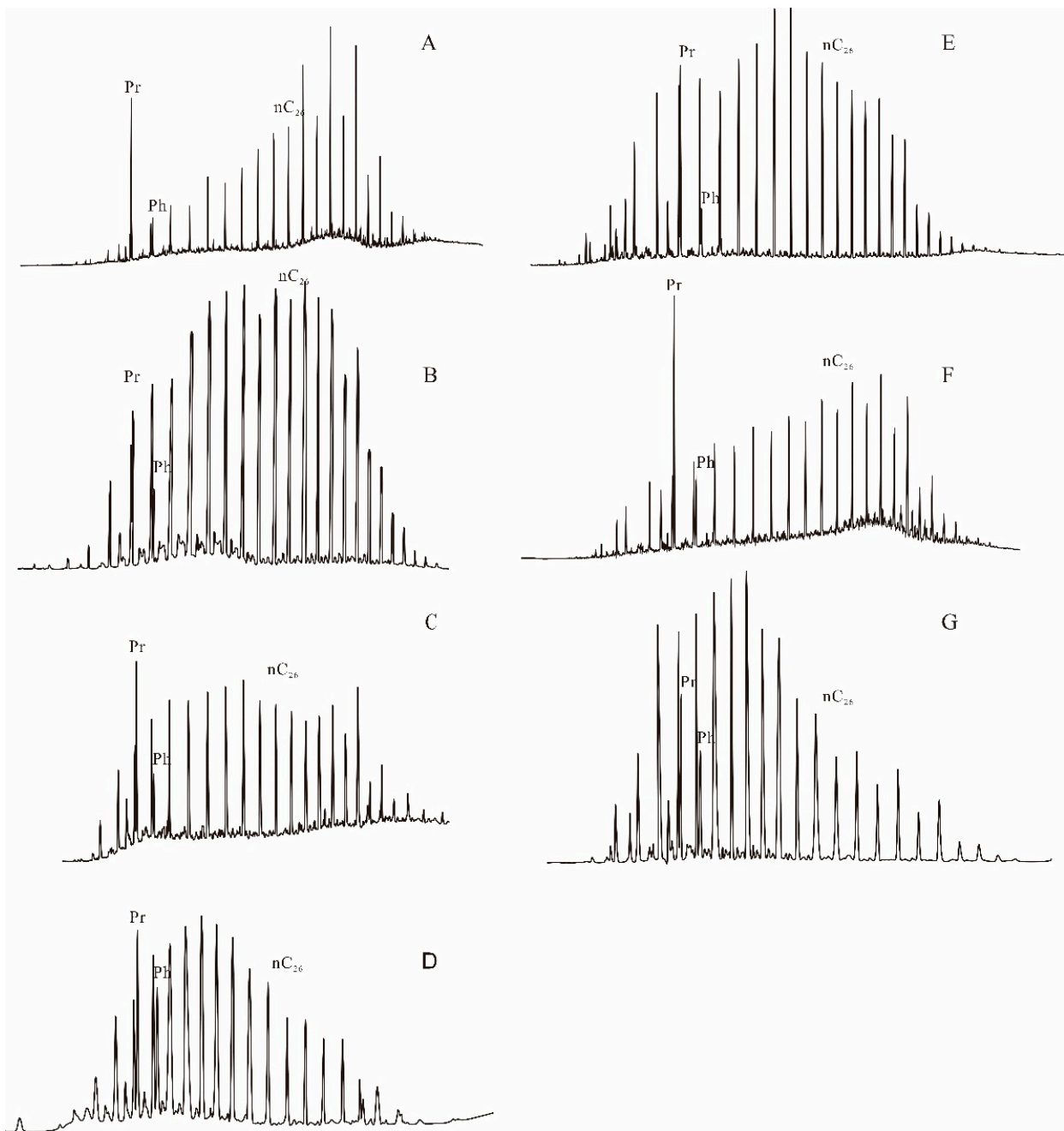
Figure 4. (**A**) Mass chromatograms of the n-alkanes (m/z 85) of the saturated hydrocarbons in Well A; (**B**) mass chromatograms of the n-alkanes (m/z 85) of the saturated hydrocarbons in Well B; (**C**) mass chromatograms of the n-alkanes (m/z 85) of the saturated hydrocarbons in Well C; (**D**) mass chromatograms of the n-alkanes (m/z 85) of the saturated hydrocarbons in Well D; (**E**) mass chromatograms of the n-alkanes (m/z 85) of the saturated hydrocarbons in Well E; (**F**) mass chromatograms of the n-alkanes (m/z 85) of the saturated hydrocarbons in Well F; (**G**) mass chromatograms of the n-alkanes (m/z 85) of the saturated hydrocarbons in Well G.

Table 1. Selected biomarker parameters for the Lingfeng Formation samples.

Well	Depth (m)	TOC (%)	C_{19}/C_{23} TT	C_{20}/C_{23} TT	C_{24} TeT/C_{23} TT	C_{27}/C_{27-29} S	C_{29}/C_{27-29} S	Pr/Ph	C_{35} H/C_{34} H	Tm/C_{30} H	Gam/C_{30} H	Ts/Tm	Ole/C_{30} H	Paq	ACL	nC_{27+29}/nC_{31+33}	$nC_{15+17+19}/nC_{27+29+31}$
A	2370	1.07	0.4	0.6	0.93	0.31	0.41	1.91	/	0.46	0.15	0.29	0.11	0.41	27.74	1.47	0.9
	2880	1.32	0.64	0.84	1.27	0.33	0.47	4.77	/	0.69	0.06	0.06	0.07	0.95	24.58	1.28	5.91
	3000	1.28	0.2	0.43	1.22	0.35	0.45	3.99	0.48	0.6	0.08	0.07	0.17	0.33	28.04	1.25	0.18
	3010	1.51	0.39	0.72	1.24	0.31	0.49	4.52	0.51	0.7	0.08	0.06	0.11	0.27	28.35	1.21	0.13
	3135	2.42	0.33	0.39	1	0.25	0.56	3.93	0.21	0.68	0.09	0.07	0.11	0.31	28.13	1.39	0.14
	3192	1.76	0.17	0.32	0.26	0.27	0.53	2.78	0.34	0.54	0.08	0.08	0.1	0.33	28.02	1.42	0.13
	2850	1.5	0.12	0.63	0.97	0.38	0.37	1.27	0.52	0.2	0.21	0.74	0.08	0.46	27.3	2	1.11
	2945	1.25	0.08	0.39	0.83	0.37	0.38	1.21	0.63	0.23	0.17	0.73	0.09	0.54	27.06	2.15	2.01
	3040	1.06	0.15	0.24	0.87	0.35	0.39	1.32	0.52	0.22	0.22	0.54	0.08	0.54	27.04	2.25	1.9
B	3235.5	0.85	0.56	0.71	0.95	0.58	0.3	2.92	0.49	0.17	0.04	0.61	0.05	0.67	26.42	2.63	1.88
	3333	1.04	1.12	1.21	1.51	0.45	0.35	3.18	0.41	0.14	0.03	0.71	0.08	0.7	26.23	3	1.96
	3347.8	1.03	0.83	1.06	1.18	0.46	0.34	2.42	0.46	0.09	0.04	1.15	0.07	0.74	26.23	2.64	2.57
	3520.5	1.02	0.41	0.98	0.64	0.59	0.29	2.28	0.61	0.33	0.11	0.24	0.01	0.63	26.75	2.26	0.71
	3616.5	1.21	0.59	0.97	0.72	0.42	0.39	2.52	0.5	0.12	0.08	1.05	0.03	0.67	26.32	2.98	1.07
	3757	1.14	0.58	0.85	0.64	0.41	0.34	2.75	0.5	0.14	0.11	0.89	0.04	0.69	26.3	2.92	1.47
C	2916.5	1.19	0.25	0.37	0.2	0.36	0.41	2.57	0.52	0.23	0.08	0.45	0.1	0.56	27.43	1.17	0.74
	3337	2.31	0.31	0.59	0.19	0.48	0.36	3.26	/	0.31	0.12	0.42	0.13	0.63	26.74	2.18	1
	3580	1.42	0.56	0.9	0.17	0.44	0.36	2.01	/	0.43	0.16	0.53	0.11	0.72	26.37	2.44	1.65
	3605	1.51	0.82	0.94	0.17	0.41	0.39	1.07	/	0.74	0.15	0.22	0.09	0.7	27.01	1.15	1.54
	3365	1.64	0.39	3.44	0.58	0.41	0.38	0.63	0.48	0.27	0.15	0.55	0.13	0.51	27.05	2.29	0.55
	3575	1.43	0.35	0.5	0.35	0.36	0.39	1.81	0.33	0.31	0.2	0.45	0.08	0.58	26.95	1.98	0.83
D	2298	0.99	0.86	0.86	0.71	0.54	0.26	3.42	0.53	0.16	0.03	0.58	0.03	0.56	26.6	3.28	0.59
	3152.5	0.88	0.44	0.81	0.69	0.57	0.22	2.97	0.5	0.15	0.06	0.75	0.05	0.67	26.21	3.52	1.04
	3257.5	0.85	0.47	0.59	0.91	0.4	0.33	2.47	0.61	0.13	0.05	1.55	0.15	0.7	26.23	2.81	1.36
E	3055	0.86	0.11	0.33	0.29	0.42	0.33	1.27	0.15	0.28	0.21	0.59	0.08	0.68	26.42	2.09	0.91
	3136	0.67	0.19	0.33	0.16	0.51	0.29	1.12	/	0.39	0.16	0.83	0.08	0.81	25.49	3.56	0.63
	3337.6	1.51	0.62	0.68	0.23	0.57	0.3	3.39	/	0.17	0.11	1.25	0.25	0.55	27.05	1.89	0.64
	3339.6	1.29	0.81	0.95	0.2	0.58	0.31	3.78	/	0.15	0.12	1.5	0.41	0.57	27	1.93	0.84
	3349.4	0.86	1.09	0.82	0.18	0.62	0.28	3.69	/	0.16	0.13	1.38	0.31	0.6	26.84	1.9	0.78
	3388	0.84	0.22	0.29	0.29	0.42	0.35	1.76	0.62	0.23	0.21	0.91	0.07	0.58	26.74	2.3	0.87
F	2610	0.81	0.43	0.63	1.35	0.28	0.5	3.35	/	0.49	0.12	0.09	0.06	0.39	27.42	1.75	0.2
	2645	1.19	0.84	1.06	1.68	0.32	0.47	4.61	0.36	0.42	0.15	0.17	0.09	0.4	27.52	1.72	0.27
	2665	1.33	0.49	0.66	1.91	0.36	0.43	4.81	0	0.61	0.08	0.1	0.05	0.38	27.39	1.99	0.22
	2675	1.06	0.68	0.66	1.2	0.36	0.41	4.63	0.39	0.39	0.13	0.12	0.08	0.41	27.66	1.54	0.39
	2635	1.1	0.8	0.65	0.27	0.33	0.45	2.18	0.33	0.49	0.11	0.1	0.07	0.45	27.47	1.6	0.42
	2670	1.17	1.05	0.8	1.74	0.33	0.44	2.45	0.31	0.59	0.1	0.1	0.06	0.48	27.41	1.64	0.34
	2705	1.24	0.98	0.75	1.99	0.33	0.45	2.34	0.33	0.53	0.11	0.12	0.07	0.49	27.35	1.47	0.48
	2734	1.23	0.83	0.53	1.51	0.32	0.45	2.41	0.34	0.43	0.12	0.16	0.08	0.41	27.25	2.12	0.33
G	3075	0.79	0.71	0.86	1.11	0.49	0.32	3.55	0.43	0.24	0.03	0.39	0.06	0.67	26.46	2.39	1.79
	3181.5	0.65	0.92	1.19	1.21	0.6	0.31	3.41	0.7	0.24	0.03	0.42	0.07	0.72	26.04	2.86	1.56
	3588	0.55	0.53	0.75	0.67	0.54	0.28	2.62	0.5	0.09	0.04	2.71	0.14	0.74	25.98	2.62	1.97
	3372.5	0.76	1.2	1.5	1.21	0.57	0.22	3.57	0.31	0.51	0.05	0.29	0.13	0.77	25.72	3.22	2.49
	3489	0.87	1.02	1.26	1.02	0.58	0.24	3.27	0.3	0.66	0.04	0.13	0.07	0.71	26.15	2.95	1.68

TT: tricyclic terpanes; TeT: tetracyclic terpanes; C_{27}/C_{27-29} S: C_{27}/C_{27-29} sterane; C_{29}/C_{27-29} S: C_{29}/C_{27-29} sterane; Pr/Ph: pristane/phytane; C_{35}/C_{34} H= C_{35} 22 S/C_{34} 22 S hopane; Ts: C_{27} 22,29,30-trisnorneohopane; Tm: C_{27} 22,29,30-trisnorhopane; Gam/C_{30} H: gammacerane/$\alpha\beta$-C_{30} hopane; Ole: oleanane; Paq: $(nC_{23} + nC_{25})/(nC_{23} + nC_{25} + nC_{29} + nC_{31})$; ACL: $(23 \times nC_{23} + 25 \times nC_{25} + 27 \times nC_{27} + 29 \times nC_{29} + 31 \times nC_{31} + 33 \times nC_{33})/(nC_{23} + nC_{25} + nC_{27+}nC_{29} + nC_{31} + nC_{33})$.

4.3.2. Terpanes

As shown in Table 1 and Figure 5, the predominance of C_{30} hopane is displayed on the m/z 191 chromatograms. The source rock m/z 191 chromatograms of the Lingfeng For-mation show the development of $C_{19\ C20\ C23}$ tricyclic terpanes (TT) and C_{24} tetracyclic terpane (TeT). The C_{19} TT/C_{23} TT C_{20} TT/C_{23} TT C_{24} TeT/C_{23} TT ratios were calculated. The C_{24} TeT/C_{23} TT of the delta front subfacies samples are 0.83–1.51, with an average of 1.31 (Table 1). The C_{24} TeT/C_{23} TT of the shallow marine subfacies samples are 0.16–1.51, with an average of 0.9 (Table 1). The C_{19} TT/C_{23} TT values of the delta front subfacies samples are 0.08–1.09, with an average of 0.5 (Table 1). The C_{19} TT/C_{23} TT values of the shallow marine subfacies samples are 0.11–1.20, with an average of 0.7 (Table 1). The gammacerane index (gammacerane/$\alpha\beta$-C_{30} ho-pane) values of the delta front subfacies source rocks are 0.06–0.22, with an average of 0.1 (Table 1). The GI values of the shallow marine subfacies source rocks are between 0.03 and 0.21, with an average of 0.1 (Table 1). The C_{35}/C_{34} H($C_{35\ 22}$ S/$C_{34\ 22}$ S hopane) ratios of the delta front subfacies source rocks are between 0.00 and 0.63, with an average of 0.3 (Table 1). The C_{35}/C_{34} H ratios of the shallow marine subfacies source rocks are between 0.15 and 0.7, with an average of 0.5 (Table 1). The oleanane index (oleanane/$\alpha\beta$-C_{30} hopane) values of the delta front subfacies source rocks are 0.05–0.41, with an average of 0.1. The oleanane index (oleanane/$\alpha\beta$-C_{30} hopane) values of the shallow marine subfacies source rocks are between 0.01 and 0.15, with an average of 0.07. The parameters of the bi-omarker compound ratios are shown in Table 1.
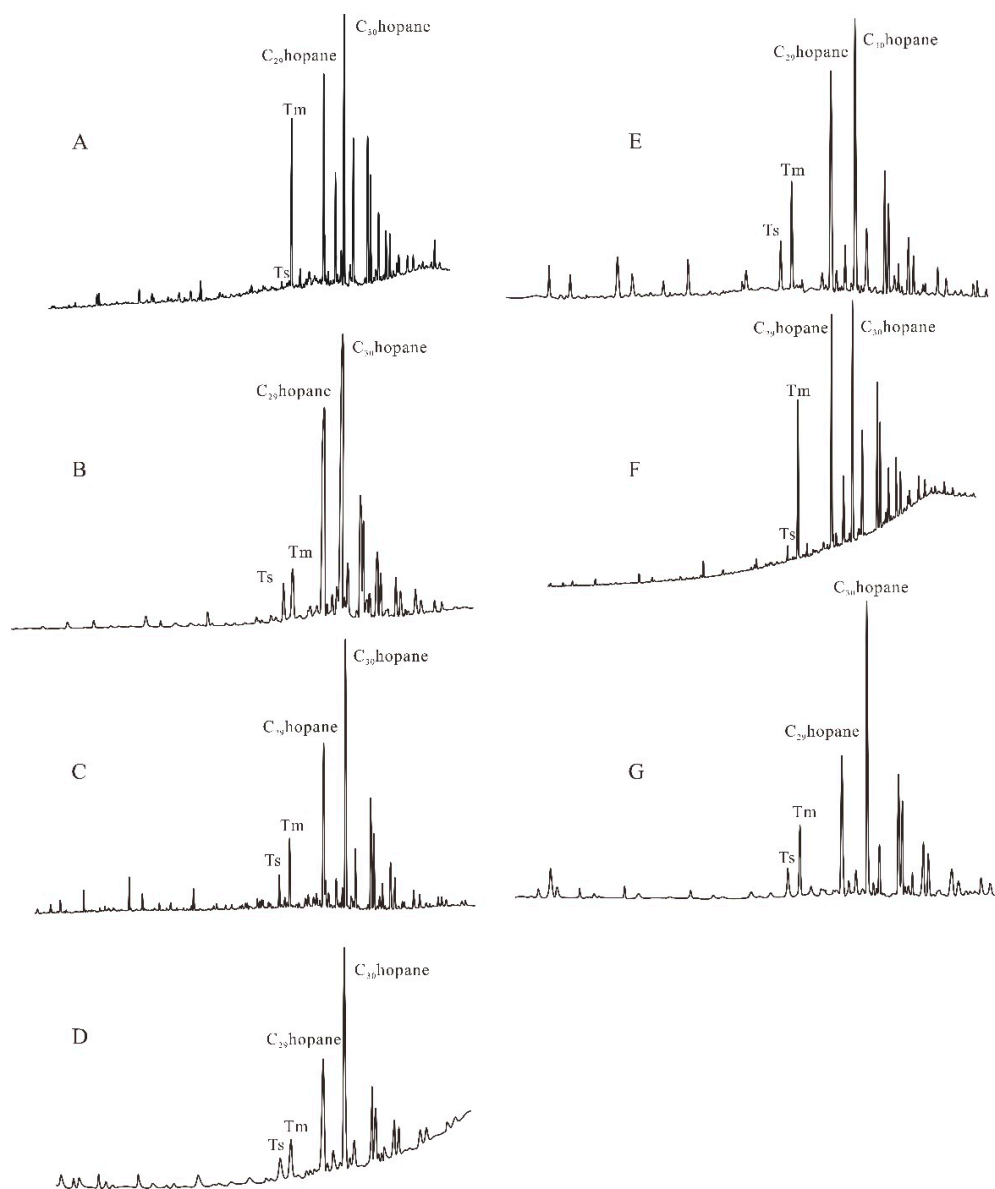
Figure 5. (**A**) Mass chromatograms of the n-alkanes (*m/z* 191) of the saturated hydrocarbons in Well A; (**B**) mass chromatograms of the n-alkanes (*m/z* 191) of the saturated hydrocarbons in Well B; (**C**) mass chromatograms of the n-alkanes (*m/z* 191) of the saturated hydrocarbons in Well C; (**D**) mass chromatograms of the n-alkanes (*m/z* 191) of the saturated hydrocarbons in Well D; (**E**) mass chromatograms of the n-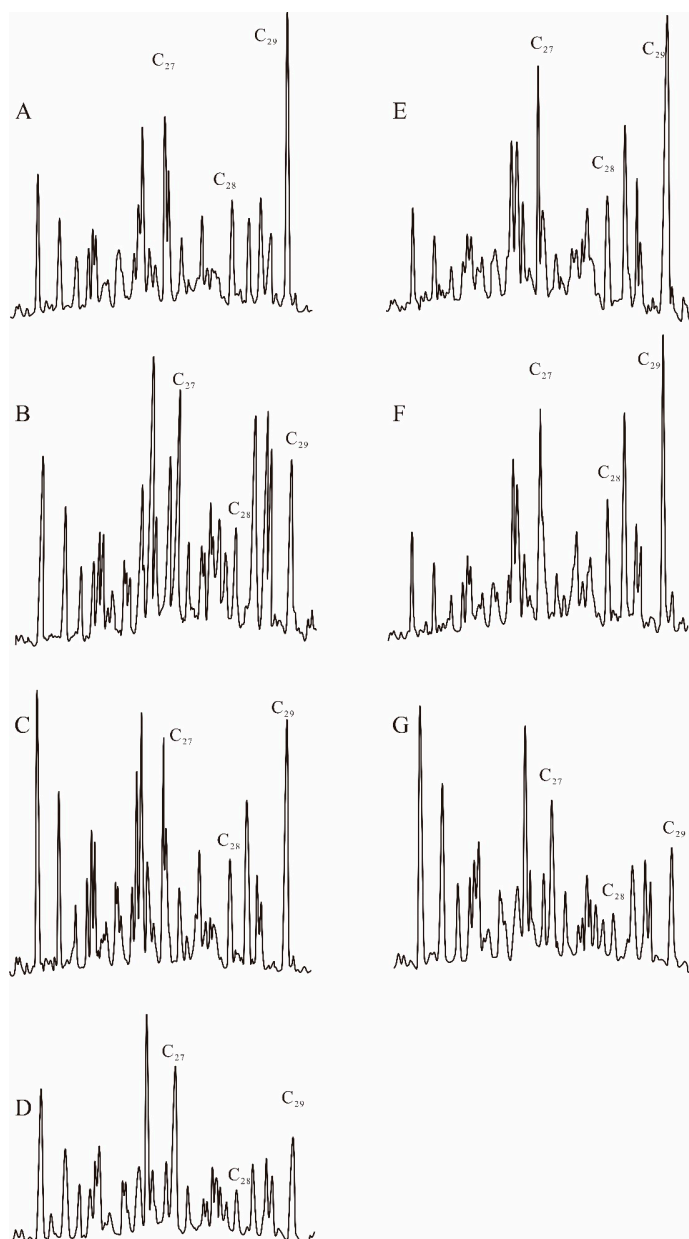alkanes (*m/z* 191) of the saturated hydrocarbons in Well E; (**F**) mass chromatograms of the n-alkanes (*m/z* 191) of the saturated hydrocarbons in Well F; (**G**) mass chromatograms of the n-alkanes (*m/z* 191) of the saturated hydrocarbons in Well G. Ts: C_{27} 22,29,30-trisnorneohopane; Tm: C_{27} 22,29,30-trisnorhopane.

4.3.3. Steranes

Considerable steranes, diasteranes and pregnanes were identified in the $m/z = 217$ mass chromatogram of all samples (Figure 6). The distribution of regular steranes in some delta front subfacies source rock (wells A and F) is dominated by an inverted "L" shape. The distribution of regular steranes in the other delta front subfacies source rock (wells C and E) is dominated by an inverted "V" shape. The distribution of regular steranes in the shallow marine subfacies source rocks (wells B, D and G) is dominated by an "L" shape. The C_{27}/C_{27-29} S ratios of the delta front subfacies samples are between 0.25 and 0.61, with an average of 0.4. The C_{27}/C_{27-29} S ratios of the shallow marine subfacies samples are

between 0.40 and 0.60, with an average of 0.51 (Table 1). The C_{29}/C_{27-29} S ratios of the delta front subfacies source rocks range from 0.28 to 0.56, with an average of 0.4 (Table 1). The C_{29}/C_{27-29} S ratios of the shallow marine subfacies samples are 0.22–0.39, with an average of 0.30 (Table 1). C_{27}, C_{28} and C_{29} rearranged steranes are widely developed in the studied samples. It is likely that the mud content was relatively high during the sedimentation period, and the clay minerals were relatively developed [45–50]. The parameters of the biomarker compound ratios are shown in Table 1.

Figure 6. (**A**) Mass chromatograms of the n-alkanes (*m*/*z* 217) of the saturated hydrocarbons in Well A; (**B**) mass chromatograms of the n-alkanes (*m*/*z* 217) of the saturated hydrocarbons in Well B; (**C**) mass chromatograms of the n-alkanes (*m*/*z* 217) of the saturated hydrocarbons in Well C; (**D**) mass chromatograms of the n-alkanes (*m*/*z* 217) of the saturated hydrocarbons in Well D; (**E**) mass chromatograms of the n-alkanes (*m*/*z* 217) of the saturated hydrocarbons in Well E; (**F**) mass chromatograms of the n-alkanes (*m*/*z* 217) of the saturated hydrocarbons in Well F; (**G**) mass chromatograms of the n-alkanes (*m*/*z* 217) of the saturated hydrocarbons in Well G.

5. Discussion

5.1. Distribution of Effective Source Rocks

Effective source rocks are defined as rocks that have generated and discharged large amounts of hydrocarbon fluids [3,22,31]. Therefore, it is important to determine effective source rocks. Because of the variations in the amount, type, and characteristics of OM found in various study regions, the criteria for effective source rocks cannot be unified. Different study areas have different standards for effective source rocks. During the production and ejection of hydrocarbons, the generated hydrocarbon should satisfy the source rock's own adsorption and then discharge the excess hydrocarbons. Therefore, before reaching source rock saturation, TOC and S_1 should have a good positive correlation. After reaching source rock saturation, with increasing TOC, S_1 tends to stabilize. Before reaching source rock saturation, TOC and S_1/TOC should have a good positive correlation, and S_1/TOC gradually increases with increasing TOC. After reaching source rock saturation, S_1/TOC gradually decreases with the beginning of hydrocarbon expulsion [21,31]. Based on this process, TOC versus S_1/TOC and TOC versus S_1 scatter plots were drawn to determine the effective source rocks of the E1l. TOC = 1.0 wt% is designated as the bottom limit of the effective source rocks. Referring to the evaluation criteria for marine source rocks proposed by scholars [21,31], TOC = 2 was defined as the lower limit of excellent source rocks. The detailed evaluation criteria are shown in Figure 7.
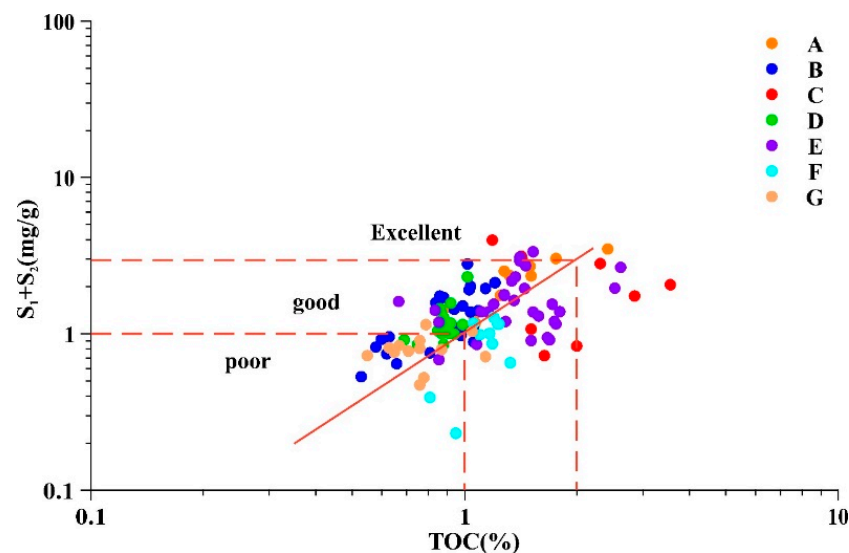

Figure 7. Cross-plot of TOC versus. $S_1 + S_2$.

According to the source rock evaluation standards, the source rocks were evaluated. The evaluation results show that the source rocks of wells A, C, E, and F are well developed. The source rocks of wells B, D, and G are poorly developed. Wells A, C, E, and F are located in the delta front subfacies, and wells B, D, and G are located in the shallow marine subfacies. The statistics show that 75% of the source rocks from the delta front facies are good source rocks, while 12% are excellent source rocks, and 81% of the source rocks from the shallow marine facies are poor source rocks, while 19% are good source rocks (Figure 8). The delta front subfacies source rocks are obviously better than those from the shallow marine subfacies.
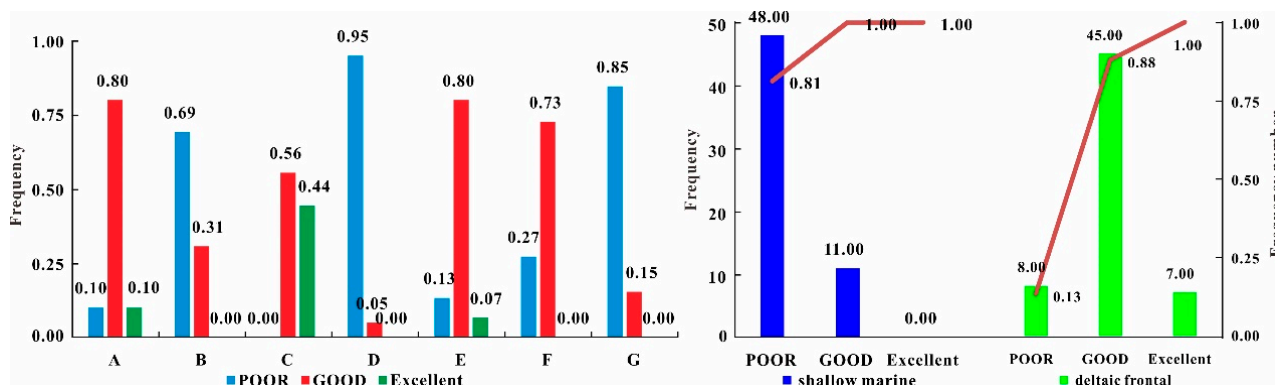
Figure 8. Source rock evaluation results.

5.2. Sedimentary Environments

The Pr/Ph reflects the redox conditions of the depositional environment [51–56]. It is generally believed that pristane and phytane are derived from phytol in chlorophyll. Phytol is converted into phytane by dehydration and hydrogenation in reducing depositional environments. Phytane is firstly oxidized to phytanic acid, and phytanic acid is converted into pristane by dehydration and hydrogenation in oxidizing depositional environments. Pr/Ph ratios of <0.6, 0.6–3.0, and >3.0 correspond to reducing, sub-reducing to sub-oxidizing, and oxidizing depositional environments, respectively [51–55,57–60]. Gammacerane is believed to be the product of the reduction of tetrahydrofuran [61]. Bacterial ciliates are thought to be precursors to tetrahydrofuran [61,62]. Bacterial ciliates generally live in the transition zone between anoxic and aerobic zones [63,64]. Therefore, the gamma wax index (GI) is used to evaluate water stratification [65]. The $C_{35}/C_{34}H$ ratio is used to indicate water salinity. Generally, the higher the salinity of the water body, the more the water body tends to restore the environment [56,66]. A graph of the relationship of each indicator was drawn. The figure shows that there is a negative correlation between GI and Pr/Ph with the R^2 of 0.29. In addition, there is a poor positive correlation between C_{35}/C_{34} H and the GI, with an R^2 of 0.06. This indicates that the GI decreases with increasing Pr/Ph ratio (Figure 9A), and the C_{35}/C_{34} H ratio increases with increasing GI (Figure 9B), which proves that these parameters are effective for evaluating the depositional environment. Each parameter indicates that the depositional environment of the delta front subfacies is generally a sub-oxidizing and oxic environment. However, due to the inconsistency between the freshwater charge of each delta and the water depth of the estuary, the water stratification and water salinity are differentiated. The shallow marine subfacies depositional environment is sub-reducing and suboxic, with a high salinity and relatively stable water stratification.

5.3. Organic Matter Sources

The short-chain n-alkanes (nC_{14}–nC_{20}) are derived from bacteria and algae, and the low-chain n-alkanes (nC_{26}–nC_{35}) are derived from terrestrial higher plants [67–70]. Terrigenous input level is calculated using the ratios $nC_{15+17+19}/nC_{27+29+31}$, nC_{27+29}/nC_{31+33}, average chain length (ACL), and aquatic microphyte (Paq), with high values of ACL indicating weak terrigenous OM input and low values of ACL indicating strong terrigenous OM input [71]. The results show that the delta front subfacies source rocks have low values of $nC_{15+17+19}/nC_{27+29+31}$, nC_{27+29}/nC_{31+33} and Paq, with high values of ACL [72,73]. In contrast, the shallow marine subfacies source rocks have high values of $nC_{15+17+19}/nC_{27+29+31}$, nC_{27+29}/nC_{31+33} and Paq and low value of ACL (Figure 10). This indicates that the delta front subfacies source rocks have source inputs mainly from terrestrial high plants, and the source of OMs of shallow marine subfacies source rocks are mainly from algae [68–70].
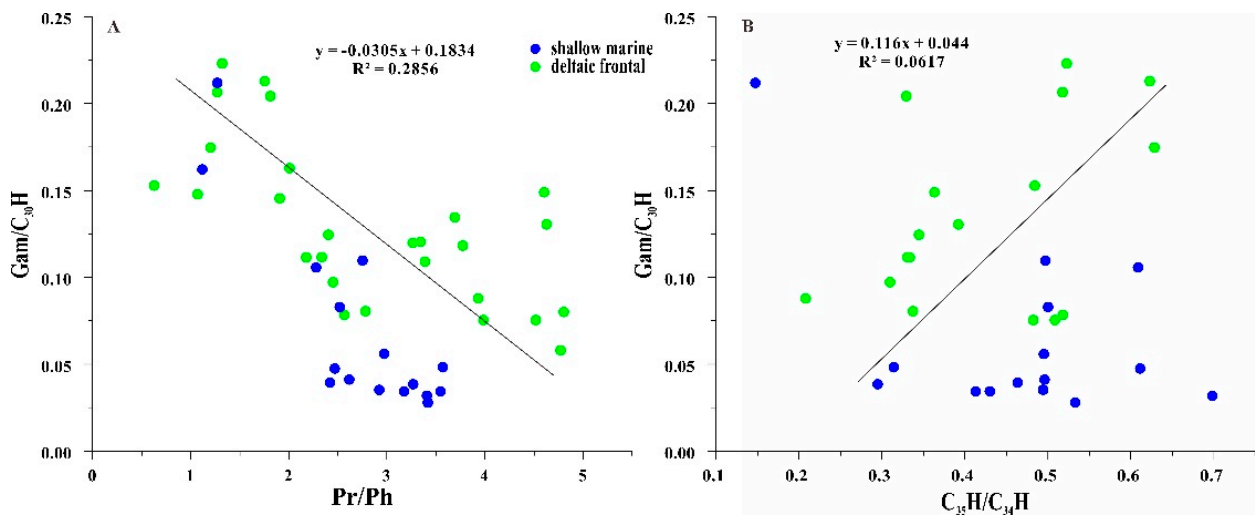
Figure 9. (**A**) The plot of the gammacerane index versus Pr/Ph; (**B**) The plot of the gammacerane index versus C_{35}/C_{34} H.
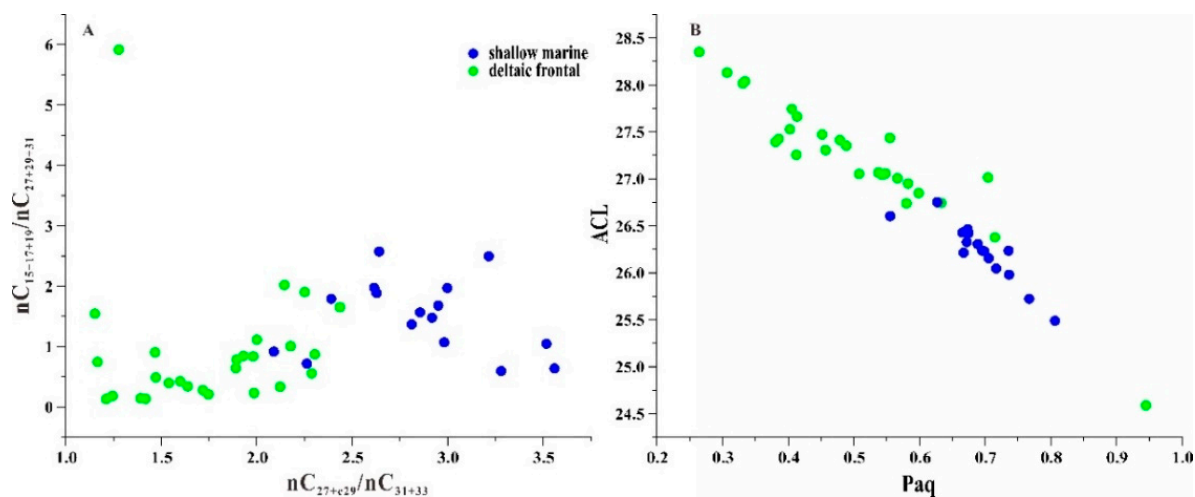

Figure 10. (**A**) The plot of $nC_{15+17+19}/nC_{27+29+31}$ versus nC_{27+29}/nC_{31+33}; (**B**) plot of Paq versus ACL.

The sources of tricyclic terpenes and tetracyclic terpenes are complex, and it is now agreed that C_{19} TT is related to the input of terrestrial higher plants, and C_{23} TT is mainly derived from aquatic organisms [74]. The C_{24} TeT is abundant in terrigenous samples [4,8,14,21,31,74]. Figure 11A shows that the delta front subfacies source rocks have high values of the two parameters, while the shallow marine subfacies source rocks have lower values. Oleanane is mainly derived from post-Cretaceous angiosperms [66,75]. The higher oleanane index values for the delta source rocks than the shallow marine subfacies source rocks suggest that the former have more angiosperm inputs than the latter (Table 1). The lower aquatic creatures and algae are the source of the C_{27} regular steranes. The regular C_{29} steranes come from higher terrestrial plants [45,48,50,76,77]. The data show that the shallow marine subfacies source rocks have a higher relative content of C_{29} regular steranes than the delta front subfacies source rocks (Figure 11B–D).
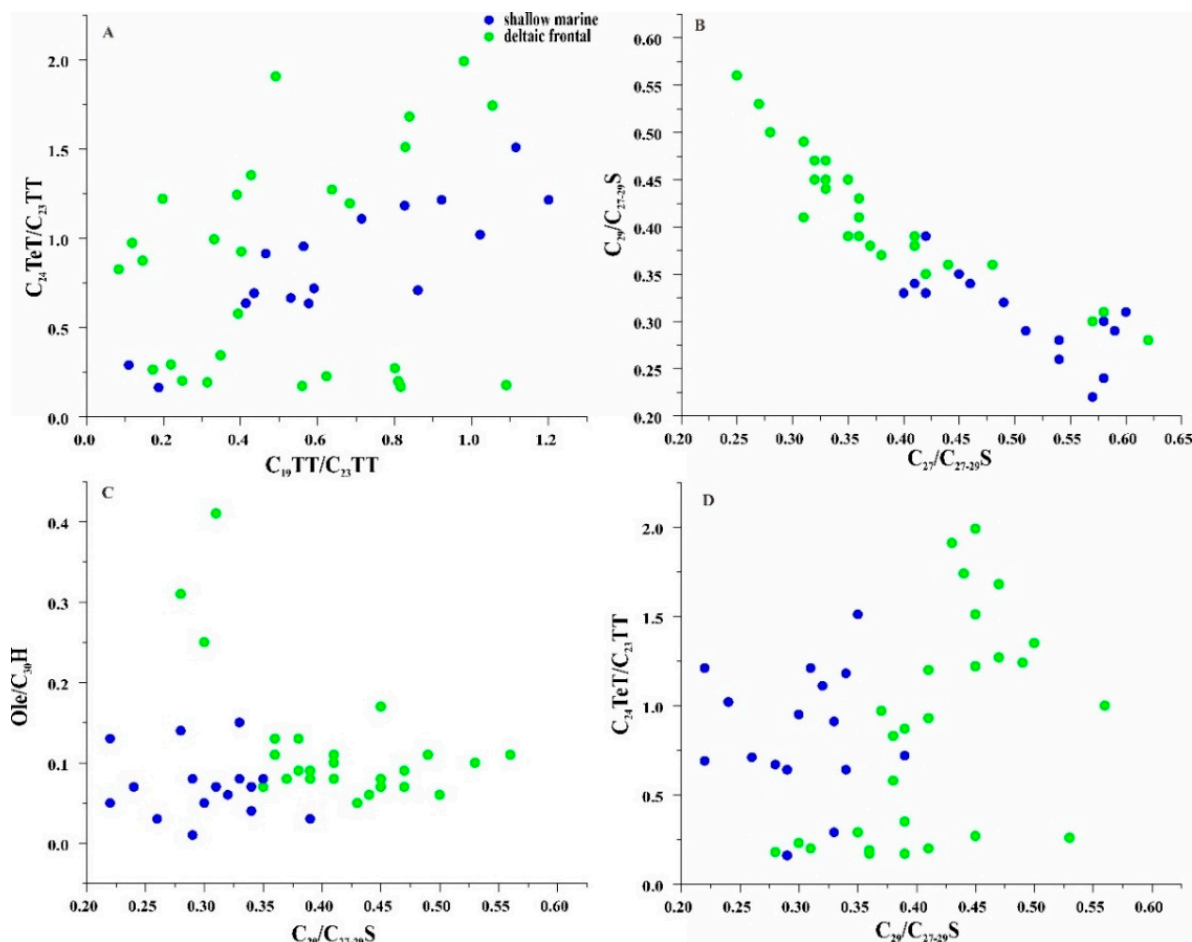
Figure 11. (**A**) The plot of C_{24} TeT/C_{23} TT versus C_{19} TT/C_{23} TT; (**B**) plot of C_{27}/C_{27-29} S versus C_{29}/C_{27-29} S; (**C**) plot of oleanane/C_{30} hopane versus C_{29}/C_{27-29} S; (**D**) plot of C_{24} TeT/C_{23} TT versus C_{29}/C_{27-29} S.

Based on the composition of n-alkanes, terpenoids and regular steranes, the OM of the delta front subfacies source rocks have source inputs mainly from terrestrial high plants; in contrast, the shallow marine subfacies source rocks have source inputs mainly from algae. The source differentiation of OM may be controlled by sedimentary facies. The delta front subfacies not only incorporates terrestrial OM input from rivers, but also in situ marine OM accumulation. The shallow marine subfacies is far from the provenance area and has a lighter input of only leaf wax, and the supply of terrigenous higher plants is poor. The algae that developed in situ are the source of OM. This development is due to the high salinity of neritic water and stable water stratification.

5.4. Organic Matter Accumulation

5.4.1. Influence of Organic Matter Input

OM input is the basic condition for OM enrichment. Marine source rocks have various sources of OM [6,7,14]. OM includes terrestrial OM debris transported by rivers, lower aquatic organisms developed in transitional facies, and planktonic algae and bacteria developed in the sea [75]. The contribution of different sources of OM to OM enrichment not only determines the pattern of OM enrichment but also controls the development location of excellent source rocks [6–8]. N-alkanes are the most abundant components in biomarker compounds [46,78–80].

Scatter plots were plotted for each biomarker parameter and TOC. The figure shows that TOC is inversely proportional to the $nC_{15+17+19}$/$nC_{27+29+31}$, nC_{27+29}/nC_{31+33} and Paq,

the R^2 values of the $nC_{15+17+19}/nC_{27+29+31}$, nC_{27+29}/nC_{31+33} and Paq are 0.14, 0.24 and 0.18 (Figure 12A–C). With increasing $nC_{15+17+19}/nC_{27+29+31}$, nC_{27+29}/nC_{31+33} and Paq, the TOC tends to increase. In addition, TOC is proportional to the ACL, with an R^2 of 0.22 (Figure 12D). As ACL increases, TOC significantly decreases.
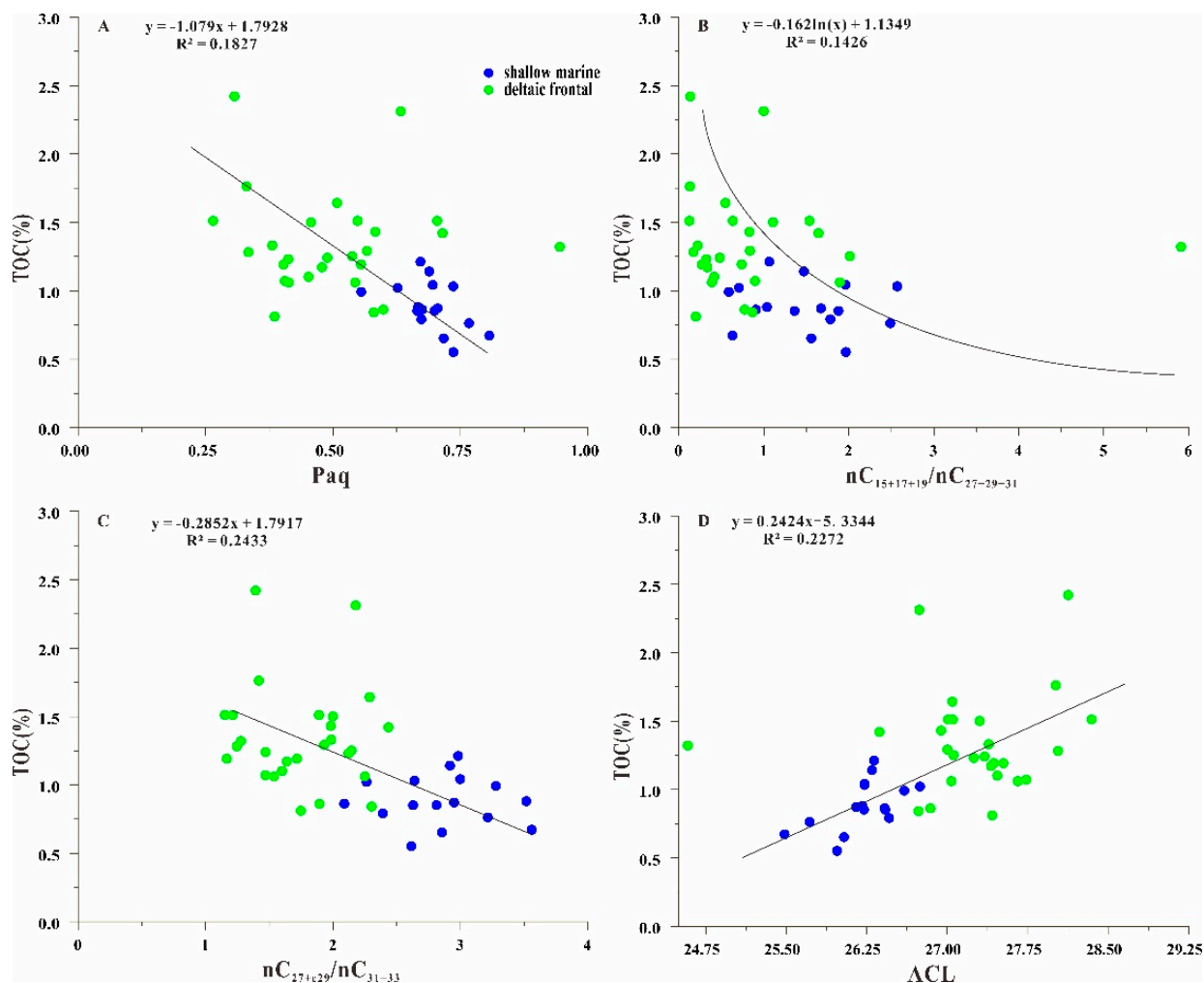

Figure 12. Relationship between OM supply index and TOC content of source rocks. (**A**) The relationship between TOC and the Paq; (**B**) relationship between TOC and the $nC_{15+17+19}/nC_{27+29+31}$; (**C**) relationship between TOC and the nC_{27+29}/nC_{31+33}; (**D**) relationship between TOC and the ACL.

The scatter plot of the C_{24} TeT/C_{23} TT ratio and TOC shows that the delta front subfacies source rocks and the shallow marine subfacies source rocks have the same characteristics. The C_{24} TeT/C_{23} TT are significantly positively correlated with TOC with the R^2 of 0.23 (Figure 13A). With increasing C_{24} TeT/C_{23} TT, the TOC tends to increase. The oleanane index and TOC have a relationship that is consistent with C_{24} TeT/C_{23} TT. There is a poor positive correlation between TOC and the oleanane index, with an R^2 of 0.11. TOC increases dramatically when the oleanane index rises (Figure 13B). The relationship between $C_{27}/C_{27–29}$ S and TOC is obviously opposite to that of $C_{29}/C_{27–29}$ S and TOC (Figure 13C,D). With increasing $C_{27}/C_{27–29}$ S, the TOC tends to decrease. With increasing $C_{29}/C_{27–29}$ S, TOC significantly increases.
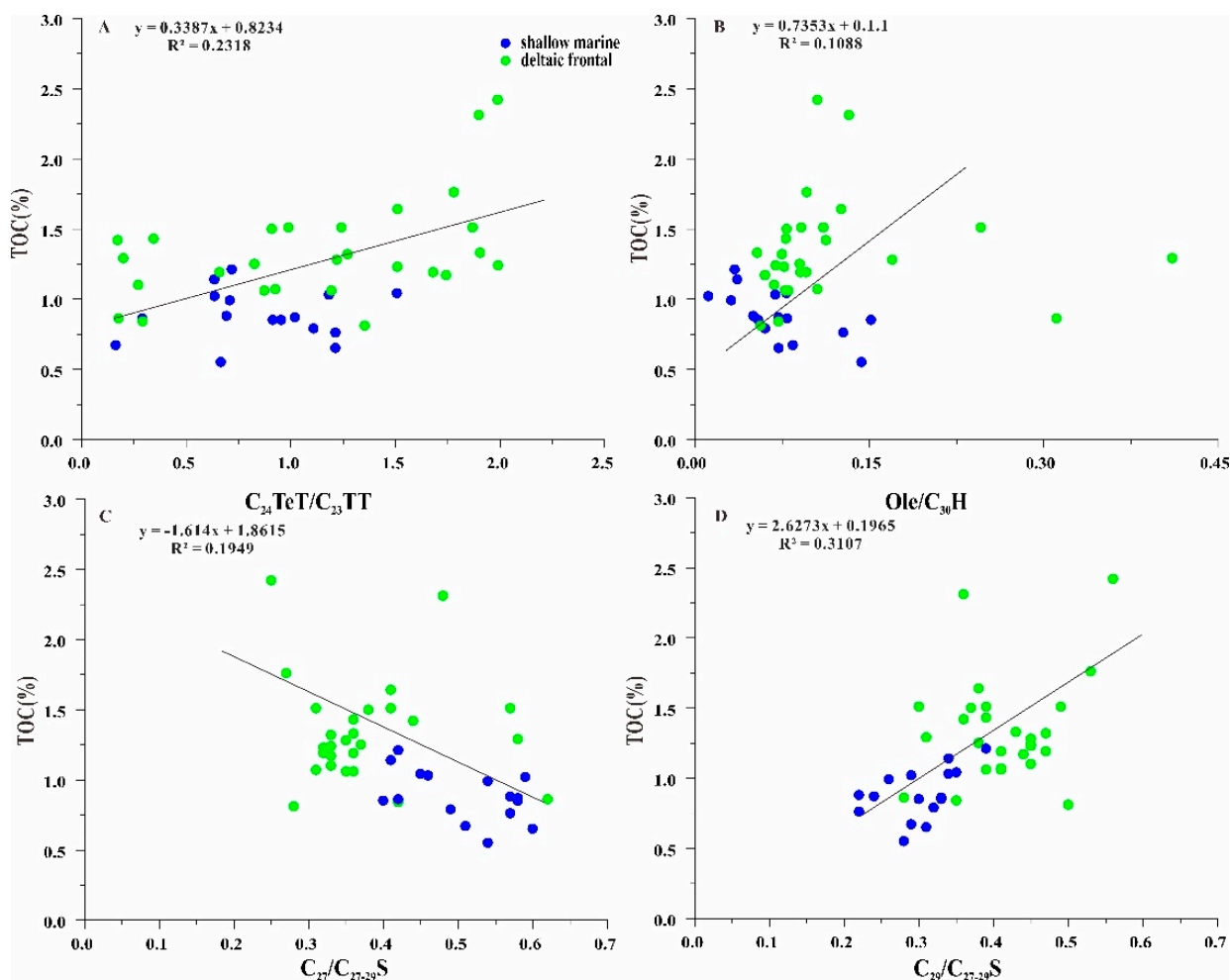
Figure 13. Relationship between OM supply index and TOC content of source rocks. (**A**) The relationship between TOC and C_{24} TeT/C_{23} TT; (**B**) relationship between TOC and oleanane/C_{30} hopane; (**C**) relationship between TOC and the regular steranes C_{27}/C_{27-29}; (**D**) relationship between TOC and the regular steranes C_{29}/C_{27-29}.

In summary, the OM enrichment of source rocks is affected by the input of terrigenous OM. The supply index of TOM ($nC_{15+17+19}/nC_{27+29+31}$, nC_{27+29}/nC_{31+33}, Paq, C_{24} TeT/C_{23} TT and C_{29}/C_{27-29} S) has a good relationship with TOC, the R^2 values of the $nC_{15+17+19}/nC_{27+29+31}$, nC_{27+29}/nC_{31+33}, Paq, C_{24} TeT/C_{23} TT and C_{29}/C_{27-29} S are 0.14, 0.24, 0.18, 0.23 and 0.31. The greater the TOM input, the greater the TOC of the source rocks. This phenomenon implies that the key element influencing the origin of the source rocks is the supply of TOM.

5.4.2. Influence of Organic Matter Preservation

OM preservation has a significant impact on the enrichment of OM. OM preservation is controlled by the redox degree of the sedimentary environment and the salinity of water [14]. OM is deactivated in oxidizing environments, which is not conducive to the preservation of OM and the origin of source rocks [14,80,81]. Scatter plots of each parameter of OM preservation and TOC were plotted. The scatter plot of Pr/Ph and TOC shows no obvious relationship between TOC and Pr/Ph (Figure 14). This phenomenon may be because when the supply of TOM is large, the environment is oxic. Furthermore, the content of original OM is high. Thus, the OM was deposited at depth and converted into excellent source rocks, even if several of the OM degraded.
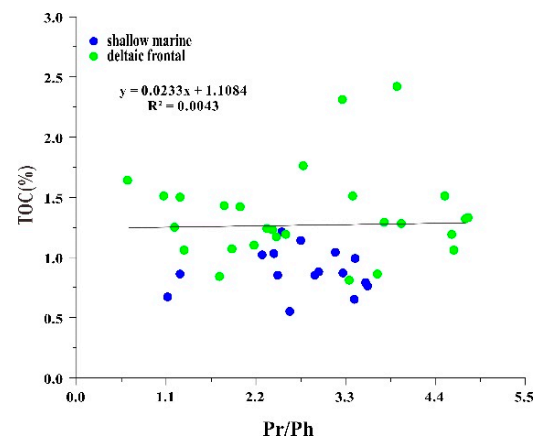
Figure 14. The relationship between the Pr/Ph and TOC.

5.4.3. Models for Effective Source Rock Formation

During the deposition of the Paleocene E1l in the Lishui Sag, the climate was warm and humid [22,31]. In addition, we identified the supply of detrital input from previous works. Li et al. pointed out that the average relative content of (Fe + K) in the E1l was 7.74% and the sediment flux in the E1l was 158 t/km^2/yr [82]. This indicates that the number of terrestrial inputs is large. Source rocks mainly developed in the delta front subfacies and shallow marine subfacies. Although the redox conditions of the delta front subfacies fluctuated greatly, the delta front consisted of a sub-oxidizing environment, providing good degradation of OM. The supply of terrigenous OM to the delta front subfacies was abundant. The amount of OM in the water is large. At the same time, the time of the exposure of OM to oxygen was reduced by the high sediment flux [1,75,82]. The OM was deposited at depth and converted into excellent source rocks. Previous works have also pointed out that TOM provided from rivers is an important factor that is critical to organic accumulation [1,35,75]. The shallow marine subfacies is far from the source supply area. Although the shallow sea subfacies redox environment was dominated by weak reduction, it was conducive to the preservation of OM. The input of TOM was small, and excellent source rocks were not developed. The input of TOM controlled the enrichment of OM in the E1l source rocks. The OM enrichment model of the E1l source rocks can be defined as the delta front-OM input type (Figure 15).
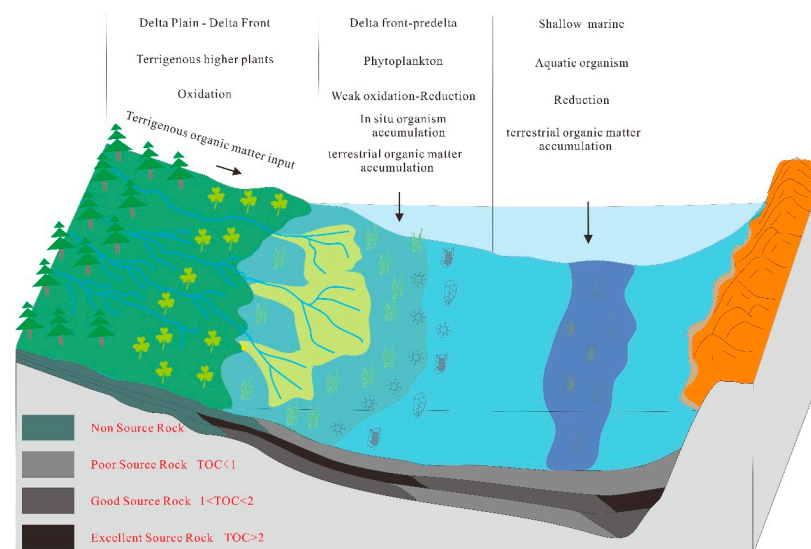

Figure 15. Organic matter enrichment model of the Lingfeng Formation source rocks.

6. Conclusions

In this study, the source rocks of the Paleocene E1l in the Lishui Sag were evaluated on the basis of TOC, rock pyrolysis and biomarker compounds. The OM source and depositional environment of the source rocks were studied. The factors controlling the variable abundance of OM in the Lingfeng Formation were studied using organic geochemical data. A model of OM enrichment was developed following examining the key variables influencing the OM input and preservation conditions. The conclusions drawn were as follows:

(1) The source rocks of the E1l had medium–high TOC (range: 0.53–3.56%, average: 1.16%). TOC = 1.0 wt% was determined as the bottom limit of the effective source rocks. TOC = 2 was determined as the lower limit of excellent source rocks. The evaluation results show that the number of excellent source rocks in the delta front subfacies was obviously greater than that in the shallow marine subfacies.

(2) Based on the data of n-alkanes, terpenoids and regular steranes, the depositional environment and OM source were analyzed. The OM in the source rocks of the delta front subfacies mainly came from terrestrial and aquatic plants, and the depositional environment consisted of oxidative–weakly reducing conditions. The OM of the shallow marine subfacies source rocks mainly came from planktonic algae, and the depositional environment consisted of weakly reducing conditions.

(3) The OM enrichment of the E1l in the Lishui Sag was controlled by the input of terrigenous OM. Terrigenous higher plants, as nutrients, promoted the accumulation of OM and the development of excellent source rocks. Preservation conditions were not the main factor controlling OM enrichment. A delta front–OM input type for the formation of these excellent source rocks is proposed.

Author Contributions: Conceptualization, X.H.; data curation, X.C. and Y.L.; formal analysis, X.H.; investigation, X.C.; methodology, X.H. and D.H.; resources, D.H.; software, Y.L.; supervision, D.H.; writing—review & editing, X.H. All authors have read and agreed to the published version of the manuscript.

Conflicts of Interest: The authors declare no conflict of interest.

References

1. Sun, R.; Li, Z.; Zhao, Z.; Yang, H.; Wang, X.; Zhao, Z. Characteristics and origin of the Lower Oligocene marine source rocks controlled by terrigenous organic matter supply in the Baiyun Sag, northern South China Sea. *J. Pet. Sci. Eng.* **2020**, *187*, 106821. [CrossRef]
2. Zhang, Y.; Sun YChen, J. Geochemical evidence of lake environments favorable for the formation of excellent source rocks: A case study from the third member of the Eocene Shahejie Formation in the Qikou Sag, Bohai Bay Basin, eastern China. *Mar. Pet. Geol.* **2022**, *136*, 105435. [CrossRef]
3. Zhu, G.-Y.; Li, T.-T.; Zhao, K.; Zhang, Z.-Y.; Chen, W.-Y.; Yan, H.-H.; Zhang, K.-J.; Chi, L.-X. Excellent source rocks discovered in the Cryogenian interglacial deposits in South China: Geology, geochemistry, and hydrocarbon potential. *Precambrian Res.* **2019**, *333*, 105455. [CrossRef]
4. Adegoke, A.K.; Abdullah, W.H.; Hakimi, M.H.; Yandoka, B.M.S. Geochemical characterisation and organic matter enrichment of Upper Cretaceous Gongila shales from Chad (Bornu) Basin, northeastern Nigeria: Bioproductivity versus anoxia conditions. *J. Pet. Sci. Eng.* **2015**, *135*, 73–87. [CrossRef]
5. Tyson, R.K. Chapter 1—History and Background. In *Principles of Adaptive Optics*; Tyson, R.K., Ed.; Academic Press: Cambridge, MA, USA, 1991; pp. 1–24.
6. Sageman, B.B.; Murphy, A.E.; Werne, J.P.; Straeten, C.A.V.; Hollander, D.J.; Lyons, T.W. A tale of shales: The relative roles of production, decomposition, and dilution in the accumulation of organic-rich strata, Middle–Upper Devonian, Appalachian basin. *Chem. Geol.* **2003**, *195*, 229–273. [CrossRef]
7. Algeo, T.J.; Kuwahara, K.; Sano, H.; Bates, S.; Lyons, T.; Elswick, E.; Hinnov, L.; Ellwood, B.; Moser, J.; Maynard, J.B. Spatial variation in sediment fluxes, redox conditions, and productivity in the Permian–Triassic Panthalassic Ocean. *Palaeogeogr. Palaeoclimatol. Palaeoecol.* **2011**, *308*, 65–83. [CrossRef]

8. Ding, X.; Qu, J.; Imin, A.; Zha, M.; Su, Y.; Jiang, Z.; Jiang, H. Organic matter origin and accumulation in tuffaceous shale of the lower Permian Lucaogou Formation, Jimsar Sag. *J. Pet. Sci. Eng.* **2019**, *179*, 696–706. [CrossRef]
9. Li, Y.; Sun, P.; Liu, Z.; Xu, Y.; Liu, R.; Ma, L. Factors controlling the distribution of oil shale layers in the Eocene Fushun Basin, NE China. *Mar. Pet. Geol.* **2021**, *134*, 105350. [CrossRef]
10. Hakimi, M.H.; Abdullah, W.H.; Alqudah, M.; Makeen, Y.M.; Mustapha, K.A. Organic geochemical and petrographic characteristics of the oil shales in the Lajjun area, Central Jordan: Origin of organic matter input and preservation conditions. *Fuel* **2016**, *181*, 34–45. [CrossRef]
11. Hakimi, M.H.; Abdullah, W.H.; Makeen, Y.M.; Saeed, S.A.; Al-Hakame, H.; Al-Moliki, T.; Al-Sharabi, K.Q.; Hatem, B.A. Geochemical characterization of the Jurassic Amran deposits from Sharab area (SW Yemen): Origin of organic matter, paleoenvironmental and paleoclimate conditions during deposition. *J. Afr. Earth Sci.* **2017**, *129*, 579–595. [CrossRef]
12. Fathy, D.; Abart, R.; Wagreich, M.; Gier, S.; Ahmed, M.S.; Sami, M. Late Campanian Climatic-Continental Weathering Assessment and Its Influence on Source Rocks Deposition in Southern Tethys, Egypt. *Minerals* **2023**, *13*, 160. [CrossRef]
13. Schubert, C.; Stein, R. Deposition of organic carbon in Arctic Ocean sediments: Terrigenous supply vs marine productivity. *Org. Geochem.* **1996**, *24*, 421–436. [CrossRef]
14. Rimmer, S.M.; Thompson, J.A.; Goodnight, S.A.; Robl, T.L. Multiple controls on the preservation of organic matter in Devonian–Mississippian marine black shales: Geochemical and petrographic evidence. *Palaeogeogr. Palaeoclimatol. Palaeoecol.* **2004**, *215*, 125–154. [CrossRef]
15. Li, W.; Zhang, Z.; Li, Y.; Fu, N. The effect of river-delta system on the formation of the source rocks in the Baiyun Sag, Pearl River Mouth Basin. *Mar. Pet. Geol.* **2016**, *76*, 279–289. [CrossRef]
16. Demaison, G. Anoxia vs. Productivity: What Controls the Formation of Organic-Carbon-Rich Sediments and Sedimentary Rocks?: Discussion (1). *AAPG Bull.* **1991**, *75*, 499.
17. Arthur, M.A.; Dean, W.E. Organic-matter production and preservation and evolution of anoxia in the Holocene Black Sea. *Paleoceanography* **1998**, *13*, 395–411. [CrossRef]
18. Zeng, S.; Wang, J.; Fu, X.; Chen, W.; Feng, X.; Wang, D.; Song, C.; Wang, Z. Geochemical characteristics, redox conditions, and organic matter accumulation of marine oil shale from the Changliang Mountain area, northern Tibet, China. *Mar. Pet. Geol.* **2015**, *64*, 203–221. [CrossRef]
19. Wu, J.; Liang, C.; Hu, Z.; Yang, R.; Xie, J.; Wang, R.; Zhao, J. Sedimentation mechanisms and enrichment of organic matter in the Ordovician Wufeng Formation-Silurian Longmaxi Formation in the Sichuan Basin. *Mar. Pet. Geol.* **2019**, *101*, 556–565. [CrossRef]
20. Hu, J.; Peng, P.; Jia, G.; Mai, B.; Zhang, G. Distribution and sources of organic carbon, nitrogen and their isotopes in sediments of the subtropical Pearl River estuary and adjacent shelf, Southern China. *Mar. Chem.* **2006**, *98*, 274–285. [CrossRef]
21. Zhang, M.; Zhang, J.; Xu, F.; Li, J.; Liu, J.; Hou, G.; Zhang, P. Paleocene sequence stratigraphy and depositional systems in the Lishui Sag, East China Sea Shelf Basin. *Mar. Pet. Geol.* **2015**, *59*, 390–405. [CrossRef]
22. Li, Y.; Zhang, J.; Shen, W.; Chang, X.; Sun, Z.; Xu, G. Organic geochemistry, distribution and hydrocarbon potential of source rocks in the Paleocene, Lishui Sag, East China Sea Shelf Basin. *Mar. Pet. Geol.* **2019**, *107*, 382–396. [CrossRef]
23. Li, Y.; Zhang, J.; Xu, Y.; Chen, T.; Liu, J. Improved understanding of the origin and accumulation of hydrocarbons from multiple source rocks in the Lishui Sag: Insights from statistical methods, gold tube pyrolysis and basin modeling. *Mar. Pet. Geol.* **2021**, *134*, 105361. [CrossRef]
24. Jiang, Z.; Li, Y.; Du, H.; Zhang, Y. The Cenozoic structural evolution and its influences on gas accumulation in the Lishui Sag, East China Sea Shelf Basin. *J. Nat. Gas Sci. Eng.* **2015**, *22*, 107–118. [CrossRef]
25. Su, A.; Chen, H.; Cao, L.; Lei, M.; Wang, C.; Liu, Y.; Li, P. Genesis, source and charging of oil and gas in Lishui sag, East China Sea Basin. *Pet. Explor. Dev.* **2014**, *41*, 574–584. [CrossRef]
26. Weilin, Z.; Kai, Z.; Xiaowei, F.; Chunfeng, C.; Minqiang, Z.; Shunli, G. The formation and evolution of the East China Sea Shelf Basin: A new view. *Earth-Sci. Rev.* **2019**, *190*, 89–111. [CrossRef]
27. Huang, Y.; Tarantola, A.; Wang, W.; Caumon, M.-C.; Pironon, J.; Lu, W.; Yan, D.; Zhuang, X. Charge history of CO_2 in Lishui sag, East China Sea basin: Evidence from quantitative Raman analysis of CO_2-bearing fluid inclusions. *Mar. Pet. Geol.* **2018**, *98*, 50–65. [CrossRef]
28. Zhao, S.; Liu, L.; Liu, N. Petrographic and stable isotopic evidences of CO_2-induced alterations in sandstones in the Lishui sag, East China Sea Basin, China. *Appl. Geochem.* **2018**, *90*, 115–128. [CrossRef]
29. Huang, Y.; Tarantola, A.; Lu, W.; Caumon, M.-C.; He, S.; Zhuang, X.; Yan, D.; Pironon, J.; Wang, W. CH4 accumulation characteristics and relationship with deep CO_2 fluid in Lishui sag, East China Sea Basin. *Appl. Geochem.* **2020**, *115*, 104563. [CrossRef]
30. Liu, L.; Li, Y.; Dong, H.; Sun, Z. Diagenesis and reservoir quality of Paleocene tight sandstones, Lishui Sag, East China Sea Shelf Basin. *J. Pet. Sci. Eng.* **2020**, *195*, 107615. [CrossRef]
31. Lei, C.; Yin, S.; Ye, J.; Wu, J.; Wang, Z.; Gao, B. Characteristics and deposition models of the paleocene source rocks in the Lishui Sag, east China sea shelf basin: Evidences from organic and inorganic geochemistry. *J. Pet. Sci. Eng.* **2021**, *200*, 108342. [CrossRef]
32. Liang, J.; Wang, H. Cenozoic tectonic evolution of the East China Sea Shelf Basin and its coupling relationships with the Pacific Plate subduction. *J. Asian Earth Sci.* **2019**, *171*, 376–387. [CrossRef]
33. Yang, C.S.; Yang, C.Q.; Shang, L.N.; Yan, Z.H.; Yang, Y.Q. Discovery of Late Cretaceous-Paleocene faulted basins developed on the Yandang Low Uplift, East China Sea Shelf Basin. *China Geol.* **2019**, *2*, 243–244. [CrossRef]

34. Zhu, X.; Wang, L.; Zhou, X. Structural features of the Jiangshao Fault Zone inferred from aeromagnetic data for South China and the East China Sea. *Tectonophysics* **2022**, *826*, 229252. [CrossRef]

35. Fu, C.; Li, S.; Li, S.; Xu, J.; Huang, Y. Genetic types of mudstone in a closed-lacustrine to open-marine transition and their organic matter accumulation patterns: A case study of the paleocene source rocks in the east China sea basin. *J. Pet. Sci. Eng.* **2022**, *208*, 109343. [CrossRef]

36. Peters, K.E. Guidelines for Evaluating Petroleum Source Rock Using Programmed Pyrolysis. *AAPG Bull.* **1986**, *70*, 318–329.

37. Tang, Y.; Zhang, J.; Li, M.; Liu, Y.; Li, M.; Sun, P. Origin of crude oils from the paleogene Xingouzui formation in the Jiangling depression of Jianghan basin, central China. *J. Pet. Sci. Eng.* **2020**, *195*, 107976. [CrossRef]

38. Xu, M.; Hou, D.; Lin, X.; Liu, J.; Ding, W.; Xie, R. Organic geochemical signatures of source rocks and oil-source correlation in the Papuan Basin, Papua New Guinea. *J. Pet. Sci. Eng.* **2022**, *210*, 109972. [CrossRef]

39. Hu, G.; He, F.; Mi, J.; Yuan, Y.; Guo, J. The geochemical characteristics, distribution of marine source rocks and gas exploration potential in the northwestern Sichuan Basin, China. *J. Nat. Gas Geosci.* **2021**, *6*, 199–213. [CrossRef]

40. Yang, M.-H.; Zuo, Y.-H.; Yan, K.-N.; Zhou, Y.-S.; Zhang, Y.-X.; Zhang, C.-F. Hydrocarbon generation history constrained by thermal history and hydrocarbon generation kinetics: A case study of the Dongpu Depression, Bohai Bay Basin, China. *Pet. Sci.* **2021**, *19*, 472–485. [CrossRef]

41. Inan, S.; Yalçin, M.N.; Mann, U. Expulsion of oil from petroleum source rocks: Inferences from pyrolysis of samples of unconventional grain size. *Org. Geochem.* **1998**, *29*, 45–61. [CrossRef]

42. Cota, L.; Baric, G. Petroleum potential of the Adriatic offshore, Croatia. *Org. Geochem.* **1998**, *29*, 559–570. [CrossRef]

43. Altunsoy, M.; Özçelik, O. Organic facies characteristics of the Sivas Tertiary Basin (Turkey). *J. Pet. Sci. Eng.* **1998**, *20*, 73–85. [CrossRef]

44. Wang, Z.; Tang, Y.; Wang, Y.; Zheng, Y.; Chen, F.; Wu, S.; Fu, D. Kinetics of shale oil generation from kerogen in saline basin and its exploration significance: An example from the Eocene Qianjiang Formation, Jianghan Basin, China. *J. Anal. Appl. Pyrolysis* **2020**, *150*, 104885. [CrossRef]

45. Zhang, J.; Yang, Y.; Gao, Y.; Li, S.; Yu, B.; Gong, X.; Bai, Z.; Miao, M.; Zhang, Y.; Sun, Z.; et al. Geochemistry and source of crude oils in the Wensu uplift, Tarim Basin, NW China. *J. Pet. Sci. Eng.* **2022**, *208*, 109448. [CrossRef]

46. Chen, J.; Qin, Y.; Huff, B.G.; Wang, D.; Han, D.; Huang, D. Geochemical evidence for mudstone as the possible major oil source rock in the Jurassic Turpan Basin, Northwest China. *Org. Geochem.* **2001**, *32*, 1103–1125. [CrossRef]

47. Escobar, M.; Márquez, G.; Suárez-Ruiz, I.; Juliao, T.; Carruyo, G.; Martínez, M. Source-rock potential of the lowest coal seams of the Marcelina Formation at the Paso Diablo mine in the Venezuelan Guasare Basin: Evidence for the correlation of Amana oils with these Paleocene coals. *Int. J. Coal Geol.* **2016**, *163*, 149–165. [CrossRef]

48. Mukhopadhyay, P.; Goodarzi, F.; Kruge, M.; Alimi, M. Comparison of source rock geochemistry of selected rocks from the Schei Point group and Ringnes formation, Sverdrup basin, arctic Canada. *Int. J. Coal Geol.* **1997**, *34*, 225–260. [CrossRef]

49. Song, D.; Chen, Y.; Wang, T.; Li, M.; Li, P. Organic geochemical compositions of Mesoproterozoic source rocks in the Yanliao Rift, Northern China. *Mar. Pet. Geol.* **2020**, *123*, 104740. [CrossRef]

50. Chen, J. A comparative study of free and bound bitumens from different maturesource rocks with Type III kerogens. *Org. Geochem.* **2017**, *112*, 1–15. [CrossRef]

51. Abdullah, W.H. Organic facies variations in the Triassic shallow marine and deep marine shales of central Spitsbergen, Svalbard. *Mar. Pet. Geol.* **1999**, *16*, 467–481. [CrossRef]

52. Bechtel, A.; Jia, J.; Strobl, S.A.; Sachsenhofer, R.F.; Liu, Z.; Gratzer, R.; Püttmann, W. Palaeoenvironmental conditions during deposition of the Upper Cretaceous oil shale sequences in the Songliao Basin (NE China): Implications from geochemical analysis. *Org. Geochem.* **2012**, *46*, 76–95. [CrossRef]

53. Gao, G.; Titi, A.; Yang, S.; Tang, Y.; Kong, Y.; He, W. Geochemistry and depositional environment of fresh lacustrine source rock: A case study from the Triassic Baijiantan Formation shales in Junggar Basin, northwest China. *Org. Geochem.* **2017**, *113*, 75–89. [CrossRef]

54. Quan, Y.; Chen, Z.; Jiang, Y.; Diao, H.; Xie, X.; Lu, Y.; Du, X.; Liu, X. Hydrocarbon generation potential, geochemical characteristics, and accumulation contribution of coal-bearing source rocks in the Xihu Sag, East China Sea Shelf Basin. *Mar. Pet. Geol.* **2022**, *136*, 105465. [CrossRef]

55. Cheng, B.; Wang, T.-G.; Huang, H.; Wang, G. Application of the monoterpane ratio (MTR) to distinguish marine oils from terrigenous oils and infer depositional environment in northern Tarim Basin, China. *Org. Geochem.* **2015**, *85*, 1–10. [CrossRef]

56. Fathy, D.; Wagreich, M.; Sami, M. Geochemical Evidence for Photic Zone Euxinia During Greenhouse Climate in the Tethys Sea, Egypt. In *Advances in Geophysics, Tectonics and Petroleum Geosciences*; Meghraoui, M., Ed.; Springer International Publishing: Cham, Switzerland, 2022; pp. 373–374.

57. Didyk, B.M.; Simoneit, B.R.T.; Brassell, S.C.; Eglinton, G. Organic geochemical indicators of palaeoenvironmental conditions of sedimentation. *Nature* **1978**, *272*, 216–222. [CrossRef]

58. Adedosu, T.A.; Sonibare, O.O.; Tuo, J.; Ekundayo, O. Biomarkers, carbon isotopic composition and source rock potentials of Awgu coals, middle Benue trough, Nigeria. *J. Afr. Earth Sci.* **2012**, *66–67*, 13–21. [CrossRef]

59. Ayinla, H.A.; Abdullah, W.H.; Makeen, Y.M.; Abubakar, M.; Jauro, A.; Yandoka, B.M.S.; Mustapha, K.A.; Abidin, N.S.Z. Source rock characteristics, depositional setting and hydrocarbon generation potential of Cretaceous coals and organic rich mudstones from Gombe Formation, Gongola Sub-basin, Northern Benue Trough, NE Nigeria. *Int. J. Coal Geol.* **2017**, *173*, 212–226. [CrossRef]

60. Asi, M.O.; Adamu, C.I.; Okon, E.E.; Neji, P.A.; Nganje, T.N.; Oli, O.O.; Eneogwe, C. Hydrocarbon potentials of sediments of the Ikom-Mamfe embayment, Southeastern Nigeria and Western Cameroon. *J. Afr. Earth Sci.* **2021**, *185*, 104411. [CrossRef]

61. Damsté, J.S.S.; Kenig, F.; Koopmans, M.P.; Köster, J.; Schouten, S.; Hayes, J.; de Leeuw, J.W. Evidence for gammacerane as an indicator of water column stratification. *Geochim. Cosmochim. Acta* **1995**, *59*, 1895–1900. [CrossRef] [PubMed]

62. Pancost, R.D.; Freeman, K.H.; E Patzkowsky, M.; A Wavrek, D.; Collister, J.W. Molecular indicators of redox and marine photoautotroph composition in the late Middle Ordovician of Iowa, USA. *Org. Geochem.* **1998**, *29*, 1649–1662. [CrossRef]

63. Cheng, B.; Chen, Z.; Chen, T.; Yang, C.; Wang, T.G. Biomarker signatures of the Ediacaran–Early Cambrian origin petrolum from the central Sichuan Basin, South China: Implications for source rock characteristics. *Mar. Pet. Geol.* **2018**, *96*, 577–590. [CrossRef]

64. Li, W.; Lu, S.; Xue, H.; Zhang, P.; Wu, S. The formation environment and developmental models of argillaceous dolomite in the Xingouzui Formation, the Jianghan Basin. *Mar. Pet. Geol.* **2015**, *67*, 692–700. [CrossRef]

65. Hackley, P.C.; SanFilipo, J.R. Organic petrology and geochemistry of Eocene Suzak bituminous marl, north-central Afghanistan: Depositional environment and source rock potential. *Mar. Pet. Geol.* **2016**, *73*, 572–589. [CrossRef]

66. Li, Q.; Xu, S.; Hao, F.; Shu, Z.; Chen, F.; Lu, Y.; Wu, S.; Zhang, L. Geochemical characteristics and organic matter accumulation of argillaceous dolomite in a saline lacustrine basin: A case study from the paleogene xingouzui formation, Jianghan Basin, China. *Mar. Pet. Geol.* **2021**, *128*, 105041. [CrossRef]

67. Wang, C.; Hren, M.T.; Hoke, G.D.; Liu-Zeng, J.; Garzione, C.N. Soil n-alkane δD and glycerol dialkyl glycerol tetraether (GDGT) distributions along an altitudinal transect from southwest China: Evaluating organic molecular proxies for paleoclimate and paleoelevation. *Org. Geochem.* **2017**, *107*, 21–32. [CrossRef]

68. Wang, Y.; Yang, H.; Zhang, J.; Gao, W.; Huang, C.; Xie, B. Characterization of n-alkanes and their carbon isotopic composition in sediments from a small catchment of the Dianchi watershed. *Chemosphere* **2015**, *119*, 1346–1352. [CrossRef]

69. El Nemr, A.; Moneer, A.A.; Ragab, S.; El Sikaily, A. Distribution and sources of n-alkanes and polycyclic aromatic hydrocarbons in shellfish of the Egyptian Red Sea coast. *Egypt. J. Aquat. Res.* **2016**, *42*, 121–131. [CrossRef]

70. Wang, M.; Zheng, Z.; Gao, Q.; Zong, Y.; Huang, K.; Shi, S. The environmental conditions of MIS5 in the northern South China Sea, revealed by n-alkanes indices and alkenones from a 39 m-long sediment sequence. *Quat. Int.* **2018**, *479*, 70–78. [CrossRef]

71. Seki, O.; Okazaki, Y.; Harada, N. Assessment of long-chain n-alkanes as a paleoclimate proxy in the Bering Sea sediments. *Prog. Oceanogr.* **2021**, *198*, 102687. [CrossRef]

72. Zhang, Y.; Yu, J.; Su, Y.; Du, Y.; Liu, Z. A comparison of n-alkane contents in sediments of five lakes from contrasting environments. *Org. Geochem.* **2020**, *139*, 103943. [CrossRef]

73. Boreddy, S.K.; Haque, M.; Kawamura, K.; Fu, P.; Kim, Y. Homologous series of n-alkanes (C19-C35), fatty acids (C12-C32) and n-alcohols (C8–C30) in atmospheric aerosols from central Alaska: Molecular distributions, seasonality and source indices. *Atmos. Environ.* **2018**, *184*, 87–97. [CrossRef]

74. Disnar, J.; Harouna, M. Biological origin of tetracyclic diterpanes, n-alkanes and other biomarkers found in lower carboniferous Gondwana coals (Niger). *Org. Geochem.* **1994**, *21*, 143–152. [CrossRef]

75. Xu, Z.; Wang, Y.; Jiang, S.; Fang, C.; Liu, L.; Wu, K.; Luo, Q.; Li, X.; Chen, Y. Impact of input, preservation and dilution on organic matter enrichment in lacustrine rift basin: A case study of lacustrine shale in Dehui Depression of Songliao Basin, NE China. *Mar. Pet. Geol.* **2022**, *135*, 105386. [CrossRef]

76. Hakimi, M.H.; Ahmed, A.F. Petroleum source rock characterisation and hydrocarbon generation modeling of the Cretaceous sediments in the Jiza sub-basin, eastern Yemen. *Mar. Pet. Geol.* **2016**, *75*, 356–373. [CrossRef]

77. Furmann, A.; Mastalerz, M.; Brassell, S.C.; Pedersen, P.K.; Zajac, N.A.; Schimmelmann, A. Organic matter geochemistry and petrography of Late Cretaceous (Cenomanian-Turonian) organic-rich shales from the Belle Fourche and Second White Specks formations, west-central Alberta, Canada. *Org. Geochem.* **2015**, *85*, 102–120. [CrossRef]

78. Bouloubassi, I.; Rullkötter, J.; Meyers, P.A. Origin and transformation of organic matter in Pliocene–Pleistocene Mediterranean sapropels: Organic geochemical evidence reviewed. *Mar. Geol.* **1999**, *153*, 177–197. [CrossRef]

79. Grice, K.; Schouten, S.; Peters, K.E.; Damsté, J.S.S. Molecular isotopic characterisation of hydrocarbon biomarkers in Palaeocene–Eocene evaporitic, lacustrine source rocks from the Jianghan Basin, China. *Org. Geochem.* **1998**, *29*, 1745–1764. [CrossRef]

80. Ramanampisoa, L.; Disnar, J.R. Primary control of paleoproduction on organic matter preservation and accumulation in the Kimmeridge rocks of Yorkshire (UK). *Org. Geochem.* **1994**, *21*, 1153–1167. [CrossRef]

81. Tong, X.; Hu, J.; Xi, D.; Zhu, M.; Song, J.; Peng, P. Depositional environment of the Late Santonian lacustrine source rocks in the Songliao Basin (NE China): Implications from organic geochemical analyses. *Org. Geochem.* **2018**, *124*, 215–227. [CrossRef]

82. Li, D.Y.; Jiang, X.D.; Xu, F.; Liu, J.S.; Hou, G.W. Geochemistry of the Paleocene Clastic Rocks in Lishui Sag, East China Sea Shelf Basin: Implications for Tectonic Background and Provenance. *Acta Geol. Sin.-Engl. Ed.* **2016**, *90*, 166–181.